

## EVIDENCE FOR A HEATED GAS BUBBLE INSIDE THE “COOLING FLOW” REGION OF MKW3S

P. MAZZOTTA<sup>1,2</sup>, J.S. KAASTRA<sup>3</sup>, F.B. PAERELS<sup>4</sup>, C. FERRIGNO<sup>3</sup>, S. COLAFRANCESCO<sup>5</sup>, R. MEWE<sup>3</sup>, AND  
W.R. FORMAN<sup>1</sup>

*Accepted for publication in ApJ Letters*

### ABSTRACT

We report on the deep *Chandra* observation of central  $r = 200$  kpc region of the cluster of galaxies MKW3s which was previously identified as a moderate cooling flow cluster. The *Chandra* image reveals two striking features – a 100 kpc long and 21 kpc wide filament, extending from the center to the south-west and a nearly circular, 50 kpc diameter depression 90 kpc south of the X-ray peak. The temperature map shows that the filamentary structure is colder while the surface brightness depression is hotter than the average cluster temperature at any radius. The hot and the cold regions indicate that both cooling and heating processes are taking place in the center of MKW3s. We argue that the surface brightness depression is produced by a heated, low-density gas bubble along the line of sight. We suggest that the heated bubble is produced by short-lived nuclear outbursts from the central galaxy.

*Subject headings:* galaxies: clusters: general — galaxies: clusters: individual (MKW3s) — X-rays: galaxies — cooling flows

### 1. INTRODUCTION

It has been argued that cooling flows (see Fabian 1994 for a review) are the natural state of cluster cores and that more than 40% of clusters have flows depositing more than  $100 h_{50}^{-2} M_{\odot} \text{ yr}^{-1}$  (see e.g. Peres et al. 1998). However, recent *Chandra* and XMM results have not confirmed cooling flow rates calculated from simple models. The clearest discrepancy with the “standard” cooling flow model is obtained with the XMM-RGS: the spectra from cooling flow regions in clusters show a remarkable lack of emission lines from gas with  $T \leq 1$  keV (Peterson et al. 2001, Kaastra et al. 2001, Tamura et al. 2001). To explain the observed disagreement with “simple” cooling flow expectations, the above authors propose a number of possible physical mechanisms (see also Fabian et al. 2001). One mechanism invoked to reduce the cooling rate is intracluster medium (ICM) heating by powerful radio sources (mainly AGN) in the nucleus of the central galaxy. Among the several difficulties of such a scenario is that, to date, no cluster shows the ICM heating taking place.

We present the temperature map of the central  $r = 200$  kpc region of MKW3s derived from a deep *Chandra* observation. Even though MKW3s was previously identified as a moderate cooling flow cluster ( $\dot{M} \approx 170 M_{\odot} \text{ yr}^{-1}$ , Peres et al. 1998), we argue that it shows evidence for hot gas bubbles which could be heated by AGN activity of the central galaxy. We also show evidence for a cold filament similar to that seen by *Chandra* in A1795 (Fabian et al. 2000) but we defer to a later publication (Mazzotta et al. 2001, in preparation) for a discussion.

We use  $H_0 = 50 \text{ km s}^{-1} \text{ kpc}^{-1}$ , which implies a linear scale of 1.21 kpc per arcsec at the distance of MKW3s ( $z = 0.045$ ).

### 2. CLUSTER OBSERVATIONS

#### 2.1. X-ray Imaging Analysis

MKW3s was observed on April 2000 in ACIS-I with an exposure of  $\approx 57$  ksec. We cleaned the data as in Mazzotta et al. (2001).

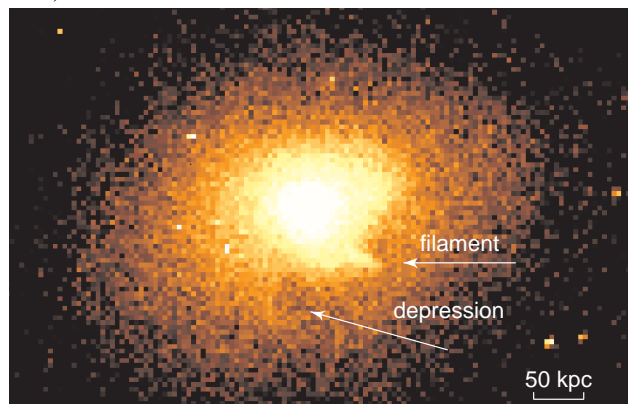


FIG. 1.— *Chandra* image of the central  $r = 200$  kpc region of MKW3s in the 0.5 – 8 keV energy band. Each pixel corresponds to  $4'' \times 4''$ . The arrows indicate the most prominent features: the filamentary structure and the surface brightness depression.

A background subtracted, vignetting corrected *Chandra* image of the X-ray emission in the 0.5 – 8 keV energy band, from MKW3s, is shown in Fig. 1. The image reveals a surface brightness filament extending from the cluster center to the south-west and a circular-like depression south of the X-ray peak. Both features are evident in the soft band (0.5 – 2 keV) as well as in the hard band (2 – 8 keV) indicating that they are produced by a significant gas density deviation rather than by excess absorption and/or gas temperature variations. The surface brightness depression lies at  $\approx 90$  kpc ( $\approx 75''$ ) from the X-ray peak and exhibits a circular shape with radius  $r \approx 25$  kpc ( $r \approx 20''$ ). To check the statistical significance of the observed depression, we extracted the count rates from a circular region

<sup>1</sup>Harvard-Smithsonian Center for Astrophysics, 60 Garden St., Cambridge, MA 02138; mazzotta@cfa.harvard.edu

<sup>2</sup>ESA Fellow

<sup>3</sup>SRON Laboratory for Space Research Sorbonnelaan 2,3584 CA Utrecht, The Netherlands

<sup>4</sup>Astrophysics Laboratory, Columbia University, 550 West 120th Street, New York, NY 10027, USA

<sup>5</sup>Osservatorio Astronomico di Roma, Via Frascati, 33, 00040, Monteporzio Italy

inscribed in the depression ( $r = 20''$ ; hereafter region S; see Fig. 2) and the count rates in two similar regions to the east and to the west of the depression. The absorbed flux from region S is  $\approx 14\%$  lower than the flux from the neighboring regions at a  $4.7\sigma$  confidence level.

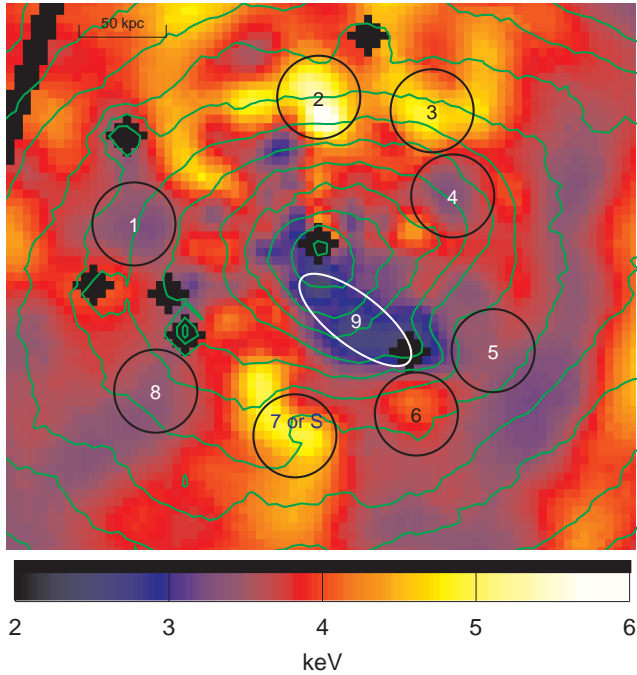


FIG. 2.— Temperature map with overlaid ACIS-I X-ray surface brightness contours (spaced by a factor of  $\sqrt{2}$ ) in the 0.5–8 keV energy band after adaptive smoothing. The black cut-out regions identify the point sources that were masked out. The statistical error in the temperature map is  $< \pm 0.4$  keV at 68% significance level ( $< \pm 0.8$  keV at 90%). The actual temperatures in the regions indicated by the cardinal numbers from 1 to 9 are reported in Fig. 3. All regions numbered 1–8 are circles with  $r = 20''$  ( $\approx 25$  kpc).

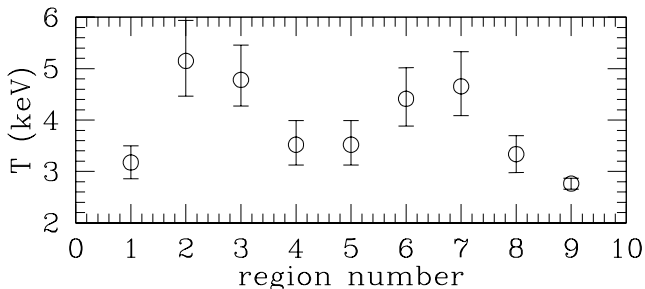


FIG. 3.— Projected emission-weighted temperature in the corresponding regions defined in Fig. 2 (error bars 90% confidence level).

## 2.2. Temperature structure

All spectral fits were made in the 0.8 – 8 keV energy band. Moreover, we multiplied the ARFs by a constant factor 0.93 for  $E < 2$  keV (Vikhlinin 2000). Each spectrum was grouped to have a minimum of 25 counts per bin and fitted with an absorbed single-temperature thermal (1-T) model (MEKAL). We fixed  $N_H$  to the Galactic value ( $N_H = 3.04 \times 10^{20} \text{ cm}^{-2}$ ) and we leave, as free parameters, the temperature, the metal abundance, and the emission measure.

Our technique for temperature map determination is the same as that in Vikhlinin, Markevitch, & Murray (2000). We extracted images in 7 energy bands (0.80 – 0.99 – 2.48 – 3.50 – 4.50 – 6.00 – 7.01 – 8.50 keV) and smoothed the images with a Gaussian filter whose width increased smoothly from  $\sigma = 4''$

at  $r = 0''$  to  $\sigma = 20''$  at  $r = 200''$ . We determined the temperature by fixing  $N_H$  at the galactic value and  $Z = 0.6 Z_\odot$  (the best-fit average of the  $r = 100$  kpc region). In Fig. 2 we overlay the X-ray contours on the temperature map. To determine the accuracy of the temperature map, we fit the X-ray spectra in 9 selected regions (indicated in Fig. 2 by numbers 1 to 9) with a 1-T model as shown in Fig. 3.

We derived the radial temperature profile of the entire cluster in twenty elliptical regions centered on the X-ray peak as shown in Fig. 4. For comparison we report the temperature profile derived from an XMM and an ASCA observation of MKW3s (Ferrigno et al. 2001, in preparation, Markevitch et al. 1998); they are in excellent agreement.

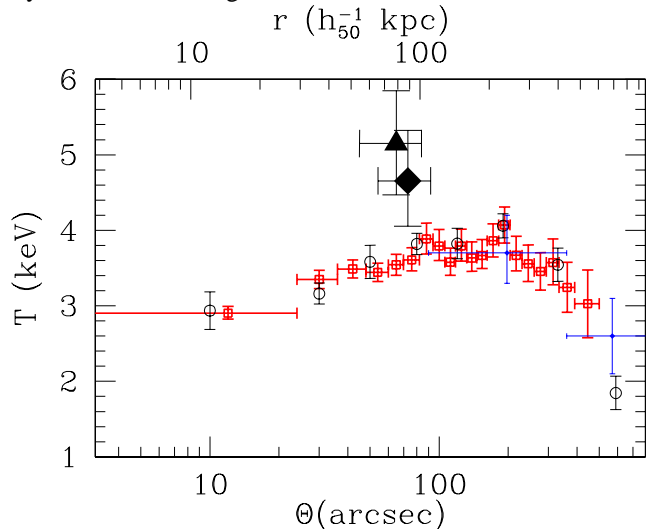


FIG. 4.— *Chandra* and XMM temperature profiles. Temperatures are extracted from ellipsoidal regions centered on the X-ray peak and oriented as the cluster surface brightness (error bars 90% confidence level). The ratio of the minor and major axes is  $\approx 0.7$ . Red crosses: temperature profile obtained from the *Chandra* observation. Black circles: temperature profile obtained from the XMM observation. Blue crosses: temperature measurements obtained from the ASCA observation. Solid diamond and triangle indicate the projected gas temperature of the region S (also 7) and 2, respectively (error bars 90% confidence level).

### 2.2.1. Temperature Structure of region S

First, we performed a variety of spectral fits to clarify the nature of the surface brightness depression. By freeing  $N_H$  in the spectral fit for the region S we find that it is consistent with the galactic value. Hence, the depression is not produced by excess absorption but rather suggests the presence of a low gas density bubble along the line of sight. Fig. 4 shows that the projected temperature of region S (solid diamond) is higher than the average temperature at any other radius.

The observed spectrum from region S may indicate either that the gas in the bubble is hotter than the ambient gas or that the emission from the bubble is dominated by a non-thermal component (e.g. a power-law). To test the origin of the emission from the depression, we fit the spectrum using two simple spectral models: an absorbed two-temperature (2-T) model and an absorbed 1-T plus a power-law model. For the first thermal component, we fixed the normalization to the estimated projected emission measure of the main cluster gas excluding a sphere of  $r_s = 25$  kpc located in the plane of the sky at 90 kpc from the cluster center. We also fixed  $N_H$  to the galactic value and the temperature of the first thermal component to  $T = 3.5$  keV, the temperature of the regions adjacent to the de-

pression. For the second component of the 2-T model, we find  $T = 7.5_{-1.5}^{+2.5}$  with  $\chi^2/(d.o.f) = 53.8/(55)$ . For the power-law model we find  $\Gamma = 1.6_{-0.2}^{+0.2}$   $k = 1.8 \times 10^{-5}$  mJy with  $\chi^2/(d.o.f) = 56.4/(55)$  (here  $S_x = k(E/1 \text{ keV})^{-\Gamma}$ ). Both models fit the observed spectrum very well.

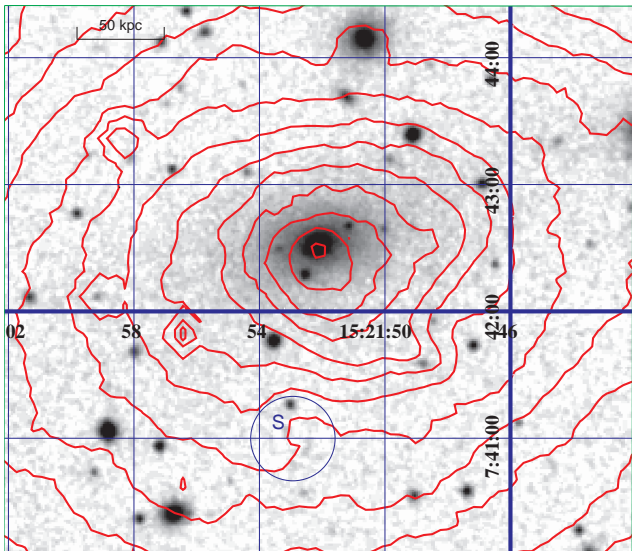


FIG. 5.— Digitized Sky Survey image with overlaid X-ray surface brightness contours as in Fig. 2. The circle identifies the region S inscribed in the X-ray surface brightness depression of Fig. 1.

### 2.3. Optical and Radio Images

In Fig. 5 we overlay the X-ray contours on the Digital Sky Survey (DSS) image. The X-ray brightness peak coincides with the optical center of the cluster cD galaxy. The optical image shows no galaxy concentration coincident with either the filament or the X-ray surface brightness depression.

In Fig. 6 we show the temperature map with overlaid VLA radio (1.4 GHz) contours. The radio image shows only two bright structures: the northern radio source is associated with the dominant cluster galaxy, the origin of the external source to the south is unclear. This source has a steep radio spectrum ( $\Gamma = 3.10$ ; De Breuck et al. 2000), but steep spectra are common both in cluster halos (see e.g. Giovannini, Tordi, & Feretti 1999) as well as in high redshift galaxies (see e.g. De Breuck et al. 2000). If it is related to the cluster, it does not coincide with either the X-ray depression or with the X-ray filament.

## 3. NATURE OF THE SURFACE BRIGHTNESS DEPRESSION

In this paper we concentrate our discussion on the nature of the X-ray surface brightness depression. In § 2.2.1 we showed that the 1-T fit to the spectrum from region S gives a temperature higher than the radially averaged gas temperature at any radius. This higher temperature may indicate either that the gas in the bubble is hotter than the ambient gas or that the bubble is dominated by non-thermal emission. Unfortunately, simple spectral analysis does not allow us to distinguish between these possibilities since both thermal and non-thermal models give acceptable fits to the observed spectrum. Thus, below we separately discuss the two possibilities and conclude that thermal emission is more likely.

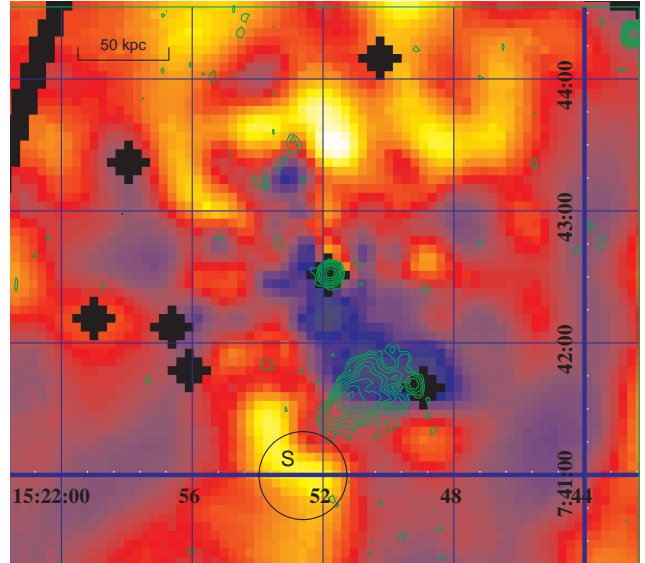


FIG. 6.— X-ray temperature map with VLA radio (1.4 GHz) contours obtained from the First Survey Catalog (contours spaced by a factor of  $\sqrt{2}$ ). The circle indicates the region S.

### 3.1. Non-thermal emission

If the emission from the bubble is dominated by a power-law component, then it may be produced by inverse-Compton (IC) scattering of a power-law distribution of relativistic electrons with the cosmic microwave background (CMB) photons (see e.g. Harris & Grindlay 1979). If this is the case we should also expect synchrotron radio emission. The radio and the X-ray fluxes provide an estimate of the magnetic field strength in the bubble (Harris & Grindlay 1979). Since the FIRST image of MKW3s shows no significant radio emission associated with the bubble, at first we assume that the radio flux  $S_r$  is equal to the survey detection limit:  $S_r(1.4 \text{ GHz}) = 1 \text{ mJy}$ . In § 2.2.1 we showed that the X-ray spectral fit gives  $S_x(1 \text{ keV}) = 1.8 \times 10^{-5} \text{ mJy}$  and  $\Gamma = 1.6$ . Using these values we find that  $B_{IC} \approx 8 \times 10^{-10} \text{ Gauss}$ . Assuming the same radio flux, we estimate the magnetic field strength using the minimum energy condition (Miley 1980) and we find  $B_{me} \approx 7 \times 10^{-5} \text{ Gauss}$ .

The two magnetic field estimates show a great discrepancy as  $B_{me}/B_{IC} \approx 8 \times 10^4$ . Because  $B_{me} \propto S_r^{0.286}$  and  $B_{IC} \propto S_r^{0.625}$ , the above discrepancy is even worse if the actual radio flux is  $S_r < 1 \text{ mJy}$ . If we believe that the minimum energy condition is valid (see e.g. Readhead 1994) then it appears unlikely that the observed X-ray emission from the bubble can be produced by IC. Moreover, from the upper limit on the radio flux, we estimate that the synchrotron energy density in the bubble is  $< 10^{-4}$  times the energy density of the CMB. Thus, we also can exclude the possibility that the observed X-ray emission is produced by the synchrotron self Compton process.

### 3.2. Thermal emission

The above considerations suggest that the emission from the low density bubble is more likely thermal. The exact determination of the gas temperature and density of the bubble depend on the actual shape and on the position of the bubble with respect to the plane of the sky. Let us assume that the bubble is a sphere and is located close to the plane of the sky. In § 2.2.1 we showed that in this case the deprojected gas temperature is  $T_b = 7.5_{-1.5}^{+2.5} \text{ keV}$ . Using the difference between the

flux in region S and the adjacent regions, we estimate the ratio  $\gamma$  between the bubble gas density  $n_b$  and the ambient gas density  $n_a$  to be  $\gamma = 0.71$ . If the bubble is at an angle  $\theta$  with respect to the plane of the sky, then the contribution of the bubble to the total flux must decrease. Thus, to obtain the observed depression, the ratio  $n_b/n_a$  must be smaller ( $\gamma < 0.71$ ). Consequently the deprojected bubble gas temperature should be  $T_b > 7.5$  keV. By requiring  $n_b > 0$  ( $\gamma > 0$ ) we can constrain the position of the bubble to  $|\theta| < 42^\circ$ . Given the density of the bubble as a function of  $\theta$ , we estimated the corresponding deprojected temperature and, thus, the pressure. By assuming that the temperature  $T_a$  of the ambient gas outside the bubble is equal to  $T_a \approx 3.5 - 4$  keV (see also Fig. 4), we find that, for  $|\theta| < 30^\circ$ , the gas pressure  $P_b$  in the bubble is 1-2 times larger than the pressure  $P_a$  of the surrounding gas. Unfortunately, for  $|\theta| > 30^\circ$  it is not possible to derive an accurate estimate of the bubble pressure as its gas density goes rapidly to zero and the resulting deprojected temperature is not constrained. The above considerations strongly suggest that the gas in the bubble was heated, started to expand (or is still expanding) and, is now (or soon will be) in pressure equilibrium with the surrounding gas.

#### 4. DISCUSSION

It is not clear how the gas inside the bubble can have been heated to such a high temperature. Nevertheless, we may expect that the bubble formed recently. If we assume that the bubble expands close to the sound speed, the bubble age is  $t \approx 2.7 \times 10^7$  yr,

much shorter than the expected age of the cluster.

The complex temperature structure and the non trivial ellipticity of the cluster core, suggest that the gas is not in hydrostatic equilibrium and/or MKW3s is undergoing a major merger. This last interpretation, however, is not supported by either the optical data or the X-ray surface brightness analysis which indicate that MKW3s is a relaxed system. Girardi et al. (1997) show that MKW3s exhibits no substructure and that the galaxy velocity distribution is Gaussian and unimodal. Moreover the velocity of the cD galaxy is consistent with the cluster mean and the velocity dispersion is consistent with the cluster mean X-ray temperature. Furthermore, the X-ray image does not show evident substructures. As shown by Buote & Tsai (1996) the power ratio  $P_2/P_0$  of the multipole terms of order 2 and 0, respectively, represent a critical indicator of the cluster dynamical status: for MKW3s, this value is consistent with

those of many relaxed systems and significantly lower of those of well known merger clusters.

One possible mechanism for heating gas in the bubble is energy injection arising from activity in the nucleus of the cD galaxy. This scenario, however, seems to be inconsistent with the radio map that shows no sign of strong nuclear activity (see § 3). However, we may be observing a cluster in which the black hole in the central galaxy undergoes short intervals ( $10^7 - 10^8$  yr) of strong activity followed by periods ( $10^9 - 5 \times 10^9$  yr) of relative quiescence (e.g. Binney & Tabor 1995, Soker et al. 2000). Such a scenario suggests that the bubble was heated during the last radio burst. If this interpretation is correct and the gas was heated by radio jets, then the hot regions on the north side of the cD galaxy (labeled as regions 2 and 3 in Fig. 2) may have been heated by a northern jet component. The fact that we do not detect a significant corresponding surface brightness depression suggests that the outburst was strongly asymmetric. Moreover, intermittent energy injection can contribute to form the observed temperature asymmetry in the core of MKW3s (see Churazov et al. 2000 for a discussion of the evolution of buoyant bubbles in cluster atmospheres).

Finally, the discovery of this heated low-density gas bubble assumes a particular importance as it clearly shows heating taking place in the cluster core region (previously identified as a cooling flow region) of an apparently “relaxed” cluster. If widespread, such gas heating mechanisms may contribute to substantially reduce the cooling rate and may explain the absence of emission lines from cool (1 keV or below) gas in recent cluster observations. Furthermore, we should expect to find them in other relaxed clusters which would clearly differentiate among the possibilities for their origin.

We thank the referee D. Buote, for useful comments and suggestions. P.M. thanks D. Harris and M. Markevitch for useful discussions. P.M. is particularly grateful to A. Vikhlinin for sharing his software tools that simplified the analysis of this *Chandra* observation. P.M. acknowledges an ESA fellowship and thanks the Center for Astrophysics for the hospitality. Support for this study was provided by NASA contract NAS8-39073, grant NAG5-3064, and by the Smithsonian Institution. The Laboratory for Space Research Utrecht is supported financially by NWO, the Netherlands Organization for Scientific Research.

#### REFERENCES

- Binney, J. & Tabor, G. 1995, MNRAS, 276, 663  
 Buote, D. A. & Tsai, J. C. 1996, ApJ, 458, 27  
 Churazov, E., Brügggen, M., Kaiser, C. R., Böhringer, H., & Forman, W. 2000, ApJ in press (astro-ph/0008215)  
 De Breuck, C., van Breugel, W., Röttgering, H. J. A., & Miley, G. 2000, A&AS, 143, 303  
 Fabian, A. C. 1994, ARA&A, 32, 277  
 Fabian, A. C., Sanders, J. S., Ettori, S., Taylor, G. B., Allen, S. W., Crawford, C. S., Iwasawa, K., & Johnstone, R. M. 2000, MNRAS, in press (astro-ph/0011547)  
 Fabian, A. C., Mushotzky, R. F., Nulsen, P. E. J., & Peterson, J. R. 2001, MNRAS, 321, L20  
 Giovannini, G., Tordi, M., & Feretti, L. 1999, New Astronomy, 4, 141  
 Girardi, M., Escalera, E., Fadda, D., Giuricin, G., Mardirossian, F., & Mezzetti, M. 1997, ApJ, 482, 41  
 Harris, D. E. & Grindlay, J. E. 1979, MNRAS, 188, 25  
 Kaastra, J. S., Ferrigno, C., Tamura, T., Paerels, F. B. S., Peterson, J. R., & Mittaz, J. P. D. 2001, A&A, 365, L99  
 Markevitch, M., Forman, W. R., Sarazin, C. L. & Vikhlinin A. ApJ 503, 77, 1998  
 Markevitch, M. et al. 2000, CXC memo (<http://asc.harvard.edu/cal/ACIS/>, “ACIS Background”)  
 Mazzotta, P., Markevitch, M., Vikhlinin, A., Forman, W. R., David, L. P., & VanSpeybroeck, L., 2001, ApJ, in press (astro-ph/0102291)  
 Miley, G. 1980, ARA&A, 18, 165  
 Peres, C. B., Fabian, A. C., Edge, A. C., Allen, S. W., Johnstone, R. M., & White, D. A. 1998, MNRAS, 298, 416  
 Peterson, J. R., et al. 2001, A&A, 365, L104  
 Readhead, A. C. S. 1994, ApJ, 426, 51  
 Soker, N., White, R. E., David, L. P., & McNamara, B. R. 2001, ApJ, 549, 832  
 Tamura, T., et al. 2001, A&A, 365, L87  
 Vikhlinin, A., 2000, *Chandra* calibration memo  
 Vikhlinin, A., Markevitch, M., & Murray, S. S. 2000, ApJ, in press (astro-ph/0008496)